Research Paper

Synergistic effect of surface and bulk single-electron-trapped oxygen vacancy of TiO_2 in the photocatalytic reduction of CO_2

Junli Li [a], Min Zhang [a], Zhongjie Guan [a], Qiuye Li [a,*], Chunqing He [b], Jianjun Yang [a,*]

[a] National & Local Joint Engineering Research Center for Applied Technology of Hybrid Nanomaterials, Collaborative Innovation Center of Nano Functional Materials and Applications of Henan Province, Henan University, Kaifeng, 475004, China
[b] School of Physics and Technology, Wuhan University, Wuhan, 430072, China

ABSTRACT

Oxygen vacancies play an important role in many photocatalytic reaction, and have attracted enormous attention from the scientists and engineers. The surface or bulk oxygen vacancies have a different function in the photo-reaction process. Herein, three different TiO_2 nanoparticles possessing surface oxygen vacancies (SO) and/or bulk single-electron-trapped oxygen vacancy (SETOV) were fabricated by dehydration or reduction of different titania precursors. The three kinds of TiO_2 nanoparticles were characterized systematically by XRD, TEM, Raman, XPS, ESR, TG, UV–vis DRS, and PL techniques. The photocatalytic reduction results of CO_2 indicated that both the bulk SETOVs and surface oxygen vacancies contributed to the enhancement of the light absorption, while the surface vacancies facilitated to the separation of the photo-generated charge carriers, and on the contrast, the bulk SETOVs acted as the recombination center. The co-existence of the surface and bulk oxygen vacancies exhibited a synergistic effect to improve the photoreduction efficiency of CO_2 to CH_4. Through adjusting the ratio of the surface and bulk oxygen vacancies and analyzing the positron lifetime and relative intensity by positron annihilation, the photoreduction efficiency of CO_2 improved with the increase of the ratio of surface oxygen vacancies to bulk SETOVs.

© 2017 Elsevier B.V. All rights reserved.

1. Introduction

As the most widely used oxide semiconductor, titanium dioxide has been widely used in photocatalytic hydrogen generation and environmental pollution elimination. While TiO_2 can only work under UV light because of its large energy band gap. For utilizing more visible light of the solar spectrum, a great deal of work by doping heteroatoms to TiO_2 has been conducted by many researchers [1–4]. Doping with foreign elements could indeed enhance the light absorption of TiO_2, but a large amount of non-intrinsic defects often generated within TiO_2 crystal lattice at the same time, and thereby the visible-light-responded photoactivity did not improved a lot although the absorption was enhanced [5,6]. In addition to the non-intrinsic defects can make the photo-response of TiO_2 red-shift, the intrinsic defects can also play the similar role, such as, Ti^{3+} ions and oxygen vacancies [7–9].

Nanotube titanic acid (NTA) is a kind of layered TiO_2-based material, and first reported in 1998 by Kasuga et al. using the concentrated alkali-thermal synthesis method [3]. It has attracted significant attention in the fields of photocatalysis, photovoltaics, nanodevices and solar cells, because of their unique structure, large BET surface areas, strong adsorption and ion-exchange capacities. In our previous study, the formation mechanism, optical and thermal property, and energy band structure of the nanotube $Na_2Ti_2O_2(OH)_2$ and $H_2Ti_2O_2(OH)_2$ have been investigated systematically and intensively [10]. NTA can transform to a novel anatase TiO_2 by thermal dehydration under high temperature treatment. This novel anatase TiO_2 is very different with the commercial or common anatase, which possesses a large amount of single-electron-trapped oxygen vacancy (SETOV, V_O) in the bulk structure, while its surface still remains the stoichiometric structure to keep them with a good stability. The concentration of $V_O^\bullet$ obtained from the hydration of NTA at 400 °C reached 4.6 $\times 10^{24}$ spin/m³ [11]. Through investigating the relationship between stokes shift and the excitation wavelength of the visible light, we found that SETOV with high concentration forms a sub-band within Eg (TiO_2). The top and bottom of the sub-band is 2.27 and 1.79 eV higher than the valence band of TiO_2, and the gap of the sub-band is 0.48 eV

* Corresponding authors.
  E-mail addresses: qiuyeli@henu.edu.cn (Q. Li), yangjianjun@henu.edu.cn (J. Yang).

[12]. This kind of novel TiO_2 (A) possesses not only a broad optical response from UV to visible light region, but also a very good chemical stability in air. Unfortunately, the visible-light-responded photoactivity of this novel TiO_2 was not good, because the sub-band formed by SETOV became the recombination of the photo-excited charge carriers [13–15].

Besides the bulk oxygen vacancies, the surface oxygen vacancies of TiO_2 also attracted much attention. As well known, when TiO_2 was treated in H_2 or other reducing ambience at high temperature, two kinds of intrinsic defects (i.e. oxygen vacancies denoted as Vo^{..}, and Ti^{3+}) would appear on TiO_2 surface simultaneously [16]. The hydrogen thermal treatment of TiO_2 nanocrystals is a simple and straightforward method to generate the surface oxygen vacancy (Vo^{..}), and the interaction of hydrogen with TiO_2 crystals has been studied for a long time [17–19]. So far, chemical reduction or oxidation, and electrochemical reduction also have been developed to synthesize the surface reduced TiO_2 nanomaterials with Vo^{..} in various sizes, shapes, and morphology [19–21]. Recently, Tan reported a facile method for production of large-scale colored TiO_2 through a controllable solid-solid reaction of $NaBH_4$ and crystalline TiO_2. The absorption of TiO_2 was enlarged into the visible-light region and the UV-light-responded photocatalytic activity of hydrogen evolution was improved apparently [22].

Based on the review of the literature, we found that both the surface oxygen vacancies and bulk SETOVs have the function of expansion of the light absorption, but they played different roles in the photocatalytic reaction. So, if both of the two kinds of vacancies coexisted in TiO_2, what's the result will happen? Herein, we designed and fabricated three different TiO_2 nanomaterials with surface oxygen vacancies and/or bulk SETOVs successfully. TiO_2 with bulk SETOVs (denoted as TiO_2-BO) was obtained by dehydration of nanotube titanic acid (NTA) at 400 °C, and the sample with surface oxygen vacancy (denoted as TiO_2-SO) was synthesized through reduction of anatase TiO_2 by $NaBH_4$, while the last one with both surface and bulk oxygen vacancy (denoted as TiO_2-SBO) was prepared by reduction of novel TiO_2 by $NaBH_4$ at high operating temperatures. The different role of the two kinds of oxygen vacancies of TiO_2 in photoreduction of CO_2 will be studied in detail. In addition, through adjusting the concentration ratio of the surface oxygen vacancies and bulk SETOVs, the possible synergistic photocatalytic mechanism of the both vacancies was proposed.

2. Experimental section

2.1. Preparation of the photocatalysts

2.1.1. TiO₂ with surface oxygen vacancies (TiO₂-SO)
Typically, 2.0 g of TiO_2 anatase nanoparticles with excess $NaBH_4$ was mixed and grounded thoroughly. Then the mixture was calcined at 350 °C for 1 h in a tubular furnace under N_2 atmosphere. After cooling down, the product was washed with deionized water and ethanol until the residual $NaBH_4$ was removed completely, and lastly dried at 70 °C [22]. And the resultant sample was denoted as TiO_2-SO.

2.1.2. TiO₂ with bulk SETOVs (TiO₂-BO)
TiO_2 with bulk SETOVs was prepared by dehydration of nanotube titanic acid (NTA) at 400 °C in air for 2 h, and NTA was synthesized by a hydrothermal method reported in our previous work [23–25].

2.1.3. TiO₂ with surface and bulk oxygen vacancies (TiO₂-SBO)
The preparation of TiO_2-SBO was prepared by calcination of TiO_2-BO and excess $NaBH_4$ with the similar method described as TiO_2-SO.

2.2. Characterization

The phase structures of the prepared photocatalysts were analyzed by X-ray diffraction (XRD) test on an X' Pert Philips diffractometer (Bruker D8 Advance). The morphologies of the samples were observed on transmission electron microscopy (TEM, JEOL JEM-2100). The ultraviolet-visible diffuse reflectance spectra (DRS) of the samples were obtained with an ultraviolet–visible spectrophotometer (UV–vis, UV-2600) using $BaSO_4$ as the reference. The photo-luminescence (PL) spectra were tested on a fluorescence spectrometer (JY HORIBA FluoroLog-3). The chemical states of the surface compositions on the catalysts were identified by X-ray photoelectron spectroscopy (XPS, AXISULTRA,) using a Kratos Axis Ultra system with monochromatic Al Ka X-rays (1486.6 eV). Electron spin resonance (ESR, Bruker E500) spectra were recorded on a spectrometer at room temperature in ambient air. The Brunauer-Emmett-Teller (BET) approach was used to evaluate the specific surface area of the samples by nitrogen adsorption-desorption test. Thermogravimetric analysis (TGA) was performed on a thermogravimetric analyzer (SDTA 851e).TGA measurements were conducted over a temperature range of 25–800 °C at a heating rate of 10 °C/min under air. Raman measurement was carried out using a Renishaw in Via Raman spectroscopy, the power of the laser was 1%, and the laser excitation was 532 nm, wavenumber range (100–800 cm^{-1}), and the exposure time was 1s. Positron annihilation lifetime spectra (PALS) were measured using a conventional ORTEC-583 fast-fast coincident system at room temperature. The coincidence spectrometer used had a prompt time resolution of 270 ps (FWHM) for the γ-rays from a ^{60}Co source selected under the experimental conditions, and the detailed measurement method was listed in the supporting information.

2.3. Evaluation of photocatalytic activity

Photocatalytic activity was conducted in a closed reactor with the inner capacity of 200 mL containing 125 mL of 0.1 mol L^{-1} $KHCO_3$ solution. 0.1 g catalyst was put into the reactor and then placed into ultrasonic to disperse the catalyst evenly. The ultra-pure gaseous CO_2 was bubbled into the solution under stirring for 1 h to obtain CO_2 saturated solution. The photocatalytic reaction was typically performed at room temperature for 6 h using a high-pressure Hg lamp (250 W), and the intensity of the light was 2.2 mW/cm². The products were analyzed by a gas chromatography (GC 9790, Zhejiang, China).

3. Results and discussion

3.1. Phase structure and morphology analysis of catalysts

The phase structure of the samples was shown in Fig. 1, and the characteristic peaks at 2θ= 25.3, 37.8, 48.1, 54.1, and 55.0° can be indexed to the (101), (004), (200), (105), and (211) crystal facets of anatase TiO_2 (PDF card 21-1272, JCPDS). From curve a and c, we can concluded that NTA has transformed to anatase TiO_2 after calcined at 400 °C for 2 h, and the phase structure was not influenced by the surface reduction by $NaBH_4$. Compared the XRD pattern of the three kinds of TiO_2, it is not difficult to find that the peak intensity of TiO_2-BO is much higher than that of TiO_2-SO and TiO_2-SBO, indicating that the crystallinity of TiO_2 with the bulk SETOVs is much better than that of the others. From our previous work, we know that the surface of TiO_2 containing bulk SETOVs still remains the stoichiometric structure [25]. And the abundant oxygen vacancies on the surface of TiO_2 would lead the disorder of the surface structure [26,27], so the peak intensity of the XRD pattern of TiO_2-SO and TiO_2-SBO is much weaker than that of TiO_2-BO.

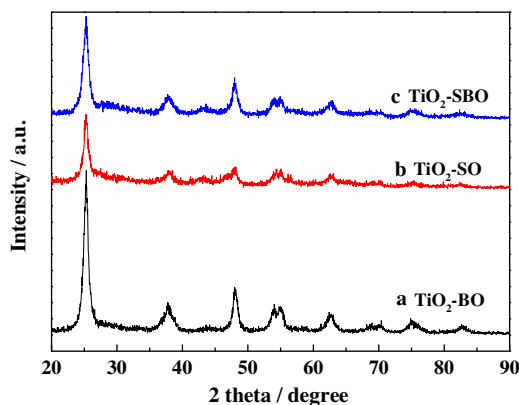**Fig 1.** XRD pattern of TiO$_2$-BO, TiO$_2$-SO and TiO$_2$-SBO.

Fig. 3. Raman spectra of TiO$_2$-BO, TiO$_2$-SO and TiO$_2$-SBO.

The morphologies of the three different TiO$_2$ were illustrated in Fig. 2. Fig. 2a showed that most of TiO$_2$-BO obtained by NTA dehydration still kept the nanotubelar morphology. The high resolution TEM in Fig. 2d showed that the lattice growth striation was clear, and the distance of lattice space was 0.35 nm, which was indexed to (101) facet of anatase TiO$_2$. Fig. 2b showed that the average particle size of TiO$_2$-SO was ca. 8–10 nm, and a thin disordered layer of 1–2 nm appeared on the surface of nanoparticles in Fig. 2e. Many literatures reported that when a large amount of surface oxygen vacancies existed on the surface of TiO$_2$, a disordered layer would appear in HRTEM observation [28,29]. So the HRTEM images of TiO$_2$-SO demonstrated that surface oxygen vacancies indeed formed on the surface of TiO$_2$ after being reduced by NaBH$_4$. Furthermore, Fig. 2c and f displayed that TiO$_2$-SBO also kept excellent nanotubelar morphology, and a similar phenomenon as well as TiO$_2$-SO was appeared, that a disordered layer of 1–2 nm existed on the surface of TiO$_2$ nanotubes. At the same time, the clear lattice growth striation was same with that of the TiO$_2$-BO. The above results illustrated that a large amount of the surface oxygen vacancy existed on the surface of TiO$_2$-SO and TiO$_2$-SBO.
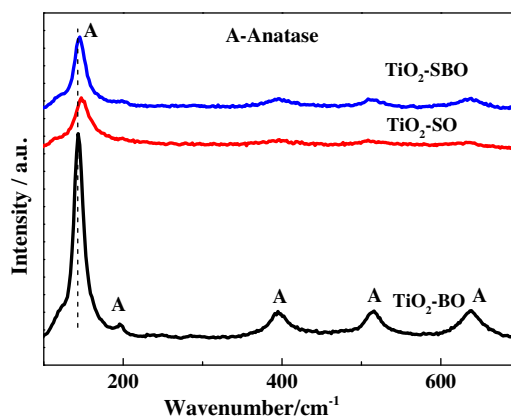
The Raman spectra in Fig. 3 showed five Raman active modes with frequencies at 144, 197, 399, 514, and 640 cm^{-1}, which indicated that all of the three samples exhibited a typical anatase phase. As is known, Raman scattering is a local probe which is very sensitive to crystallinity and microstructure. Therefore, the shift and broadening of Raman peaks of TiO$_2$-SO and TiO$_2$-SBO indicates that the original symmetry of the TiO$_2$ lattice has been broken. As reported in the previous literature [30], the shift and broadening of the peaks of TiO$_2$ were ascribed to the crystal domain size and nonstoichiometry. We can also clearly find that the peak intensity of TiO$_2$-SO and TiO$_2$-SBO obviously decreased, which were the characteristics of the existence of the disordered phase on the surface [31,32]. These results are consistent well with the observation in HRTEM images and XRD results.

3.2. XPS, ESR and TGA analysis

The bonding environment of Ti and O atoms was analyzed by X-ray photoelectron spectroscopy (XPS). As shown in Fig. 4, the spectrum of Ti2p was consisted of two individual peaks at 459.0 eV and 464.7 eV respectively, which was indexed to Ti2p3/2
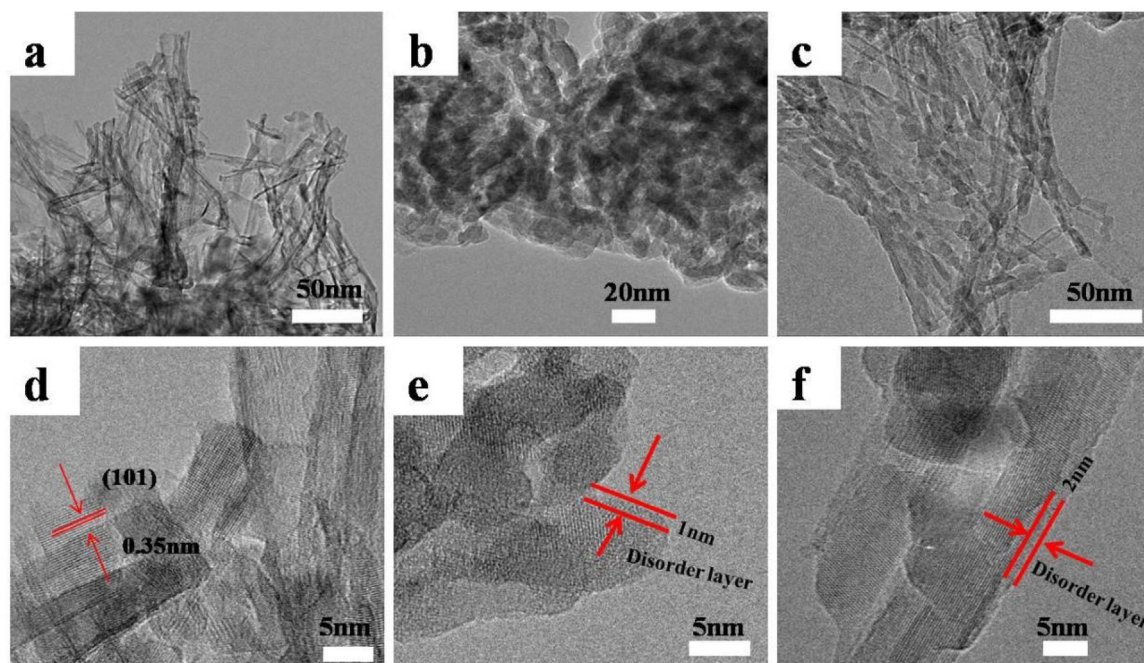

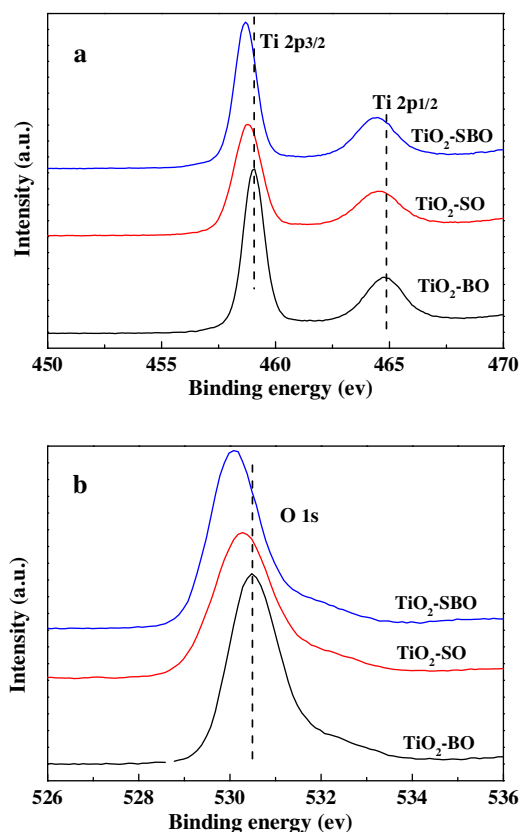**Fig. 2.** TEM and HRTEM images of TiO$_2$-BO (a, d), TiO$_2$-SO (b, e), and TiO$_2$-SBO (c, f).

Fig. 4. XPS spectra of Ti2p peaks (a) and O1 s peaks (b) for the TiO$_2$-BO, TiO$_2$-SO and TiO$_2$-SBO.

Fig. 5. ESR spectra of the TiO$_2$-SBO.

Fig. 6. TGA curves of TiO$_2$, TiO$_2$-SO (a) and TiO$_2$-BO, TiO$_2$-SBO (b) in air atmosphere.

and Ti2p1/2 binding energies, consisted well with the typical characteristics of the Ti-O-Ti bonds in TiO$_2$ [33]. The Ti2p peaks of TiO$_2$-SO shifted to low binding energies of 458.8 and 464.5 eV, while that of TiO$_2$-SBO shifted more to 458.7 and 464.4 eV, respectively. That indicated some Ti^{3+} ions may have been formed in the samples of TiO$_2$-SO and TiO$_2$-SBO [34]. The residual NaBH$_4$ would decompose under high temperature treatment and formed a reduced atmosphere, resulting in the formation of oxygen vacancy and Ti^{3+} on the surface of TiO$_2$ nanocrystals. This change in the oxidation state is supported by the observed peak shift for Ti2p to low binding energy direction. In addition, O1 s binding energy (Fig. 4b) of TiO$_2$-SBO (530.1 eV) was also lower than that of TiO$_2$-SO (530.3 eV) and TiO$_2$-BO (530.5 eV). These results indicated that the formation of some Ti^{3+} ions indeed influence the bond interaction states of Ti-O bond. Besides the XPS measurement, the electron spin resonance (ESR) spectra was also used to analysis the Ti^{3+} and oxygen vacancies.

As well known, ESR is a kind of spectrum technique to detect and study the paramagnetism materials containing unpaired electrons. Under the reduced atmosphere, the formed oxygen vacancies on the surface of TiO$_2$ often possesses two electrons (V$_O$..) or no electron (V$_O$), both of these two oxygen vacancies have no signals in ESR detection. Only the oxygen vacancies with one electron (V$_O$) would have the ESR signal. As shown in Fig. 5, two peaks was appeared in the ESR spectrum of TiO$_2$-SBO, the one of g = 1.983 was assigned to a paramagnetic Ti^{3+} center [35], and the other one of g = 2.003 was ascribed to the bulk SETOVs. Although the surface oxygen vacancies can't be detected by ESR directly, the surface oxygen vacancies often have two electrons, and some of them will reduce the adjoining Ti^{4+} to Ti^{3+}, so the formation of Ti^{3+} verified the existence of surface oxygen vacancies indirectly. The inset illustration shows a symmetrical ESR signal with g = 2.003 (G = 3508), indicated that TiO$_2$-BO only
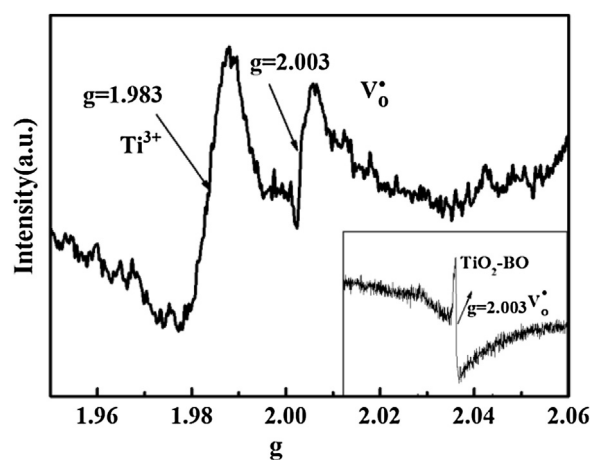
exists bulk SETOVs, that was consistent with our previous work [21–24].

In order to further understand the existence of bulk and surface oxygen vacancies, the thermogravimetric analysis (TGA) was used to detect the mass change of samples in air atmosphere. As shown in Fig. 6a, the mass loss of TiO$_2$ in the low temperature range is mainly ascribed to the desorption of physically adsorbed H$_2$O and hydroxyl groups [36]. And after that, the mass remained constant until the temperature exceeded 560 °C. Compared the two curves in Fig. 6a, we found that the curve of TiO$_2$-SO is the same as that of TiO$_2$ below 440 °C, and there is an obvious difference in mass loss between them when the temperature exceeds 440 °C. A light mass increase was observed for TiO$_2$-SO, which is finished at ca. 800 °C. There existed a large amount of oxygen vacancies on the surface of
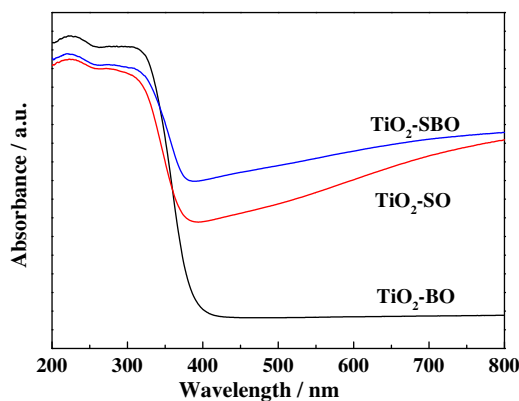
Fig. 7. The UV–vis diffuse reflection spectroscopy (DRS) of TiO_2-BO, TiO_2-SO, and TiO_2-SBO.

TiO_2-SO, so the unsaturated surface would be compensated by the oxygen when the sample was heated in air [37], and thus the mass would increase. The same phenomenon was appeared in Fig. 6b, the mass decreased first because of desorption physically adsorbed H_2O and hydroxyl groups, and increased a little at the high temperature range. Compared with TiO_2-BO, the mass increase of TiO_2-SBO was more apparently, indicating that the oxygen compensation for the surface oxygen vacancies was much easier.

3.3. Optical absorption properties

Fig. 7 shows the UV–vis diffuse reflection spectroscopy of the three kinds of TiO_2 with different oxygen vacancies. All of them have the similarly strong absorption in the UV region, but their visible light absorption has a large difference. The sample of TiO_2-BO showed a very weak absorption in the range of 400–430 nm. From our previously work, we knew that TiO_2 obtained by dehydration of NTA possessed a large amount of single electron oxygen vacancies (SETOVs), and which can form a sub-band in the forbidden band of TiO_2, and leading a visible light absorption, but the absorption intensity was relatively low [25]. And this kind of SETOV have been detected by ESR measurement, so the weak absorption of TiO_2-BO in the visible light should be attributed to the existence of SETOV. On the contrast, both TiO_2-SO and TiO_2-SBO with the surface oxygen vacancies exhibited a much stronger absorption in the visible light region of 400–800 nm. Comparing the three samples, the difference of TiO_2-BO with the others is that the latter two contains abundant surface oxygen vacancies, indicating that the surface oxygen vacancies contributed a lot to the visible light absorption. Moreover, observation of the color of the three TiO_2, we found that TiO_2-BO showed the light grey color, and the others displayed a very dark blue color. These optical colors consisted very well with the light absorption property of these three kinds of TiO_2. In addition, the colored TiO_2 samples almost scarcely change under ambient conditions over a year, implying that they showed a very long-term stability.

3.4. Photo-reduction of CO_2 to CH_4 on different TiO_2

The photoreduction of CO_2 was used as the probe reaction to evaluate the photoactivity of these three kinds of TiO_2 with different oxygen vacancies. Firstly, a series of comparison experiments was conducted to verify the photocatalytic reduction process of CO_2. When the reaction was kept in dark or without TiO_2 input, there was no CH_4 detectable, indicating that the photo-excitation of the photocatalysts was essential in CO_2 photoreduction.

The production rate of CH_4 by CO_2 photoreduction on different TiO_2 was shown in Fig. 8. Fig. 8a illustrated the photoactivity
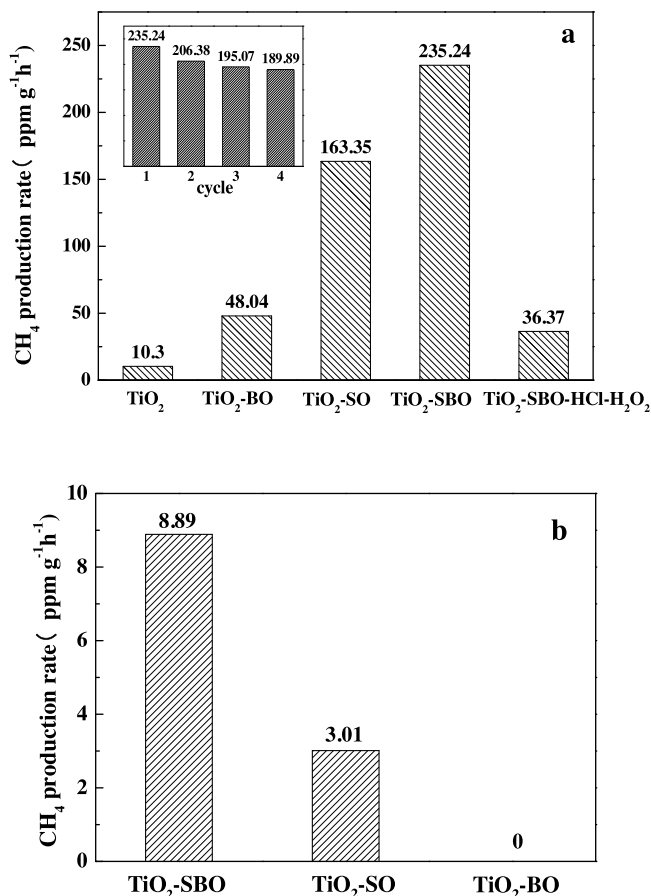

Fig. 8. Photocatalytic activity of CH_4 production rate on different TiO_2 (a: under UV irradiation, b: under visible light irradiation), the insert figure shows the stability of TiO_2-SBO.

of different kinds of TiO_2 under UV light irradiation, and the production rate of CH_4 on the common anatase TiO_2 raw was 10.30 ppm g^{-1} h^{-1}. Although TiO_2 can be excited by UV light, if there existed not any surface state to accelerate the separation of the excited charge carriers, its photoactivity was very low. However, all of TiO_2 samples containing oxygen vacancies exhibit a much higher total CH_4 production rate than the raw TiO_2. The production rate of CH_4 on TiO_2-BO was 48.04 ppm g^{-1} h^{-1}, which was much lower than that of TiO_2-SO and TiO_2-SBO. On one hand, the light absorption of TiO_2-BO was much weaker than the others. On the other hand, the large amount of bulk SETOVs in TiO_2-BO can act as the recombination center of the photoexcited charge carriers, and thus lead to a lower photoactivity of TiO_2-BO for CO_2 reduction. Comparing the photoactivities of TiO_2-SO and TiO_2-SBO, we found that the highest activity of 235.24 ppm g^{-1} h^{-1} without loading any noble metal was obtained by the latter one. Through the above analysis of the structure and morphology of these two kinds of TiO_2, we knew that both the surface oxygen vacancies and bulk SETOVs contributed to the enhancement of the light absorption. And both of TiO_2-SO and TiO_2-SBO contains a surface disordered layer corresponded to the abundant surface oxygen vacancies. According to the literature [38], the surface oxygen vacancies can acted as the separation center for the photoexcited charge carriers, so their photoactivity was much higher than TiO_2-BO. For verify the separation role for the photoexcited charge carriers, the surface oxygen vacancies was removed by hydrogen peroxide [20]. The detailed process was ascribed as that, TiO_2-SBO was added into the hydrochloric acid solution and stirred mildly for 12 h, during which 40 mL hydrogen peroxide was added, and after centrifugation, washing and drying,
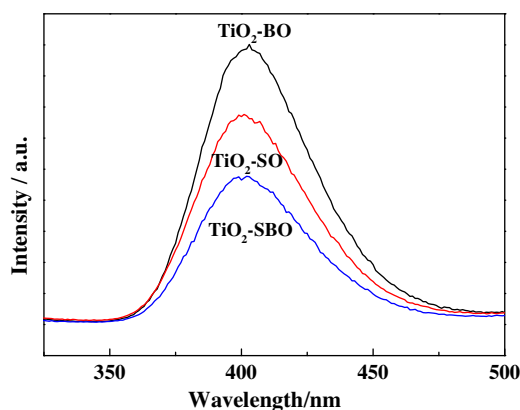
Fig. 9. The photoluminescent spectra of the TiO_2-BO, TiO_2-SO and TiO_2-SBO.

a laurel-green sample was obtained eventually. When the surface oxygen vacancies of TiO_2-SBO was removed, the photo-production rate of CH_4 decreased dramatically to 36.37 ppm g^{-1} h^{-1}, and this is almost consistent with the photoactivity of TiO_2-BO. That verified the surface oxygen vacancies indeed played a very important role in the separation efficiency for the photo-excited electron hole pairs. Moreover, the recycle experiments of TiO_2-SBO with two kinds of vacancies were conducted and shown in the inserted Fig. 8a. The production rates of CH_4 in the consecutive four cycles were 235.24, 206.38, 195.07, and 189.89 ppm g^{-1} h^{-1}, respectively. That is to say, the photoactivity kept over 81% after four recycles, indicating the sample maintained a long-term stability in the photoreduction of CO_2. In addition, the black blue color of the samples was unchanged over one year after they were synthesized (Fig. S1).

The visible-light-responded photoactivity of CO_2 reduction was also tested and shown in Fig. 8b. TiO_2-BO did not exhibit any activity under visible light irradiation. As described above, the bulk SETOV not only acted as the drawboard for the visible light, but also acted as the recombination center for the excited charge carriers, so not any activity was obtained on TiO_2-BO. The highest production rate of CH_4 was also achieved as 8.89 ppm g^{-1} h^{-1} on TiO_2-SBO, which was in accordance with the activity order under UV light irradiation. Comparison the photoactivity of TiO_2-SO, we found that the production rate of CH_4 decreased from 163.35 to 3.01 ppm g^{-1} h^{-1} when the incident light changed from full spectrum light to the visible light. The latter one is only 1.8% to the former one. And the activity of TiO_2-SO is almost 16 times of that of the common TiO_2. The biggest difference of the two sample of TiO_2-SO and pure TiO_2 is that the former one has a strong absorption of the visible light and contains a large amount of surface oxygen vacancies. Since the visible light activity of TiO_2-SO is much lower, the surface oxygen vacancies should be contributed a lot to the full spectrum activity, indicating that the surface oxygen vacancies played a very important role in separation of the photo-generated charge carriers. Let's compare the full spectrum light and visible light activity of TiO_2-SBO, the latter is 3.8% of the former, which improved a lot than the sample of TiO_2-SO. That's to say, the bulk SETOVs also contributed the visible light activity. As analyzed above, the bulk SETOVs in the forbidden band of TiO_2-SBO leads a strong visible light absorption. When the sample was excited, more photons can be utilized, and

Table 1
Positron Lifetime and Relative Intensities of TiO_2-SBO-400, TiO_2-SBO-500, TiO_2-SBO-600.

sample	τ_1 (ps)	τ_2 (ps)	I_1 (%)	I_2 (%)	I_1/I_2
TiO_2-SBO-400	274	388	72.492	27.508	2.635
TiO_2-SBO-500	291	413	82.835	17.167	4.825
TiO_2-SBO-600	297	432	89.302	10.5	8.347

so a much higher activity was achieved with the synergistic effect of the charge separation function of the surface oxygen vacancies.

The photoluminescence (PL) emission spectrum was also used to understand the transfer and recombination behavior of the photo-generated charge carriers. As shown in Fig. 9, all samples exhibited a broad signal located ca. 402 nm, which resulted from the recombination of the photo-excited electrons and holes. The peak intensity of TiO_2-BO is the highest, indicating the recombination efficiency is much higher than others [39]. Our previous work has reported that the bulk SETOVs in TiO_2-BO often acted as the recombination center for the photo-excited charge carriers, so its PL emission intensity is much higher. While the PL peak of TiO_2-SO has an obvious decrease compared with that of TiO_2-BO, which was attributed to the existence of the surface oxygen vacancies. And for TiO_2-SBO, the peak decreased further, indicating that the separation efficiency improved correspondingly. And as a result, the PL emission result fitted very well with the actual photocatalytic activity.

3.5. Effect of the ratio of surface oxygen vacancies and bulk SETOVs of TiO_2-SBO on photoactivity

Since the surface oxygen vacancy and the bulk SETOV plays different roles in the photoreduction of CO_2, the effect of the ratio of these two defects was investigated. From our previously work, the concentration of bulk SETOVs depended on the dehydration temperature of NTA [25]. Herein, the formation condition of the surface oxygen vacancies was kept unchanged, and the concentration of the bulk SETOVs was adjusted by changing the calcination temperature (400, 500, 600 °C) of NTA. Three samples with different ratio of surface oxygen vacancy and bulk SETOV were denoted as TiO_2-SBO-400, TiO_2-SBO-500, and TiO_2-SBO-600. Positron annihilation is a well-established technique to study defects in materials, so it was used to analyze the oxygen defects in TiO_2-SBO (Table 1). The longer lifetime components (τ_2) should be arises from positrons trapped by larger size defects such as oxygen vacancy clusters (i.e., dimers, trimers, or larger). Generally, the shorter lifetime components (τ_1) is attributed to the free annihilation of positrons in defect-free crystals [40,41]. In this work, the bulk SETOVs possesses one single electron, which has been verified by ESR measurement and fitted well with our previous work, so the shorter one (τ_1) should be corresponded to the positron lifetime in the bulk SETOVs. And the amount of surface oxygen vacancies were abundant according to the above analysis of HRTEM, XPS, ESR and TGA. At the same time, the defect center of surface oxygen vacancies often contains two electrons, and the abundant surface oxygen vacancies would gather to dimers, trimers, or clusters, so the longer one (τ_2) should refer to the positron lifetime in the surface oxygen vacancies. As shown in Table 1, the ratio of I_1 to I_2 (I_1/I_2) for TiO_2-SBO-400, TiO_2-SBO-500, TiO_2-SBO-600 are 2.635, 4.825, and 8.347, respectively,

Table 2
The corresponding specific rate of CO_2 production on the three samples catalysts under UV irradiation.

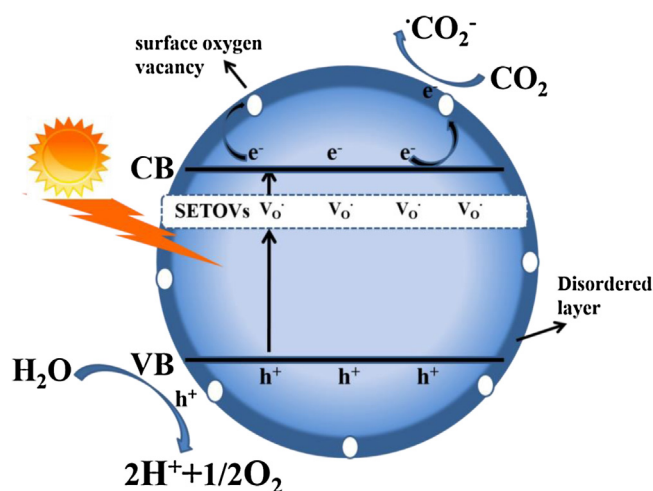| sample	surface area m^2 g^{-1}	rate of CH_4 ppm g^{-1}h^{-1}	specific rate of CH_4 ppm m^{-2} h^{-1}
TiO_2-SBO-400	202.16	235.24	1.17
TiO_2-SBO-500	138.72	139.03	1
TiO_2-SBO-600	86.19	34.4	0.4

Fig. 10. Schematic diagram of CO_2 photoreduction mechanism on TiO_2-SBO.

indicating that the ratio of bulk defects to surface defects increases with the improvement of the dehydration temperature of NTA.

The effect of defects ratio of TiO_2 nanocrystals on the photocatalytic activity of CO_2 reduction was shown in Table 2. The production rate of CH_4 on TiO_2-SBO-400, TiO_2-SBO-500, and TiO_2-SBO-600 are 235.24, 139.03, and 34.4 $ppm\,g^{-1}\,h^{-1}$, respectively. The morphology and structure of these samples is shown in Fig. S2-S5. As these three samples have different specific surface areas, their specific rates of CH_4 production (per unit surface area of catalyst) was calculated as 1.17, 1.00, and 0.40 $ppm\,g^{-1}\,m^{-2}\,h^{-1}$. In other words, increasement in the ratio of the surface oxygen vacancies leads to a significant enhancement in the photocatalytic activity. As the increase of the ratio of SO/BO, the separation efficiency of the photo-generated charge carriers would increase, and thereby improving the photocatalytic activity.

3.6. Proposal of the photocatalytic mechanism of CO_2 reduction

Based on the above experimental and discussion results, the function of oxygen vacancies of the anatase TiO_2 could be divided into three aspects: (1) TiO_2-BO possessing bulk SETOVs showed the light visible-light response, but displayed a relatively lower photocatalytic reduction activity of CO_2 to CH_4. The reason should be due to that the sub-band of TiO_2-BO formed by SETOVs acted as the drawboard to enhance the light absorption, but it also can conducted as the recombination center for the photo-generated charge carriers. (2) TiO_2-SO containing abundant surface oxygen vacancies enhanced the visible light absorption remarkably, and they are believed to act as the electron capture traps to inhibit electron–hole recombination.In addition, the surface oxygen vacancies center can also increase the adsorption for CO_2 and H_2O molecules, which will improve the photoactivity for CO_2 reduction. (3) The last TiO_2-SBO possessing simultaneously bulk SETOVs and surface oxygen vacancies can utilize the advantages of the above two kinds of TiO_2. The photocatalytic mechanism for CO_2 reduction was proposed in Fig. 10. The bulk SETOVs formed a middle band in the forbidden gap of TiO_2. When TiO_2-SBO was irradiated by the light, both of the UV and visible light can be utilized. And the surface oxygen vacancies acted as the active surface state to increase the light absorption and accelerate the separation of the photo-excited charge carriers, and thereby the photoactivity of TiO_2-SBO was highest. Therefore, the synergy effect of surface oxygen vacancies and bulk SETOVs was the main reason to response to the enhanced photoactivity.

4. Conclusions

In summary, both surface and bulk oxygen vacancies in TiO_2 nanocrystals play very important roles in photoreduction of CO_2. Three kinds of TiO_2 with different surface oxygen vacancies and bulk SETOVs was obtained, and the one possessing both defects exhibited a higher activity for CO_2 photoreduction. From the systematic analysis of the structure and properties, we knew that the bulk SETOVs formed a middle sub-band in the forbidden gap of TiO_2, and thus make TiO_2 have a response to the visible light, while they can also acted as the recombination center of the charge carriers. The surface oxygen vacancies not only have a strong response to the visible light, but also acted as the capture traps to inhibit electrons-holes recombination. By adjusting the ratio of surface oxygen vacancies and bulk SETOVs, and analyzing the lifetime and intensity by positron annihilation, the photoreduction efficiency of CO_2 improved with the increase of the ratio of surface oxygen vacancies to bulk SETOVs. The findings of this work provide fundamental insight into the role of surface/bulk defects in photocatalytic reaction and open up a novel strategy for significantly improving photocatalytic efficiency, and the strategy may also be applicable to other photocatalysts.

Appendix A. Supplementary data

Supplementary data associated with this article can be found, in the online version, at http://dx.doi.org/10.1016/j.apcatb.2017.01.025.

References

[1] S.T. Martin, C.L. Morrison, M.R. Hoffmann, J. Phys. Chem. 98 (1994) 13695–13704.
[2] O. Diwald, T.L. Thompson, T. Zubkov, E.G. Goralski, S.D. Walck, J. John, T. Yates, J. Phys. Chem. B 108 (2004) 6004–6008.
[3] Z. Shen, J. Zhong, L. Wang, Y. Zheng, Y. Cui, L. Chen, J. Mol. Catal. (China) 30 (2016) 260–268.
[4] S. Liu, J. Yu, S. Mann, J. Phys. Chem. C 113 (2009) 10712–10717.
[5] N. Serpone, J. Phys. Chem. B 110 (2006) 24287–24293.
[6] A.V. Emeline, N.V. Sheremetyeva, N.V. Khomchenko, V.K. Ryabchuk, N. Serpone, J. Phys. Chem. C 111 (2007) 11456–11462.
[7] T. Ihara, M. Miyoshi, M. Ando, S. Sugihara, Y. Iriyama, Mater. Sci. 36 (2001) 4201–4207.
[8] J. Huo, Y. Hu, H. Jiang, C. Li, Nanoscale 6 (2014) 9078–9084.
[9] J. Cai, Y. Wang, Y. Zhu, M. Wu, H. Zhang, X. Li, Z. Jiang, M. Meng, ACS Appl. Mater. Interfaces 7 (2015) 24987–24992.
[10] A. Fujishima, Nature 238 (1972) 37–38.
[11] C. Feng, Z. Jin, J. Zhang, Z. Wu, Z. Zhang, Photochem. Photobiol. 86 (2010) 1222–1229.
[12] L. Qian, Z. Jin, J. Zhang, Y. Huang, Z. Zhang, Z. Du, Appl. Phys. A 80 (2004) 1801–1805.
[13] W. Chen, X. Guo, S. Zhang, Z. Jin, J. Nanopart. Res. 9 (2007) 1173–1180.
[14] Q. Li, J. Zhang, Z. Jin, D. Yang, X. Wang, J. Yang, Z. Zhang, Electrochem. Commun. 8 (2006) 741–746.
[15] Q. Li, X. Wang, Z. Jin, D. Yang, S. Zhang, X. Guo, J. Yang, Z. Zhang, J. Nanopart. Res. 9 (2006) 951–957.
[16] X. Chen, L. Liu, F. Huang, Chem. Soc. Rev. 44 (2015) 1861–1885.
[17] T. Xia, X. Chen, J. Mater. Chem. A. 1 (2013) 2983.
[18] L. Liu, P. Yu, X. Chen, S. Mao, D. Shen, Phys. Rev. Lett. 111 (2013) 065505.
[19] J. Qiu, C. Lai, E. Gray, S. Li, S. Qiu, E. Strounina, C. Sun, H. Zhao, S. Zhang, J. Mater. Chem. A. 2 (2014) 6353.
[20] G. Zhu, Y. Shan, T. Lin, W. Zhao, J. Xu, Z. Tian, H. Zhang, C. Zheng, F. Huang, Nanoscale 8 (2016) 4705–4712.
[21] X. Zou, J. Liu, J. Su, F. Zuo, J. Chen, P. Feng, Chem. Eur. J. 19 (2013) 2866–2873.
[22] H. Tan, Z. Zhao, M. Niu, C. Mao, D. Cao, D. Cheng, P. Feng, Z. Sun, Nanoscale 6 (2014) 10216–10223.

[23] Y. Wang, C. Feng, M. Zhang, J. Yang, Z. Zhang, Appl. Catal. B- Environ. 100 (2010) 84–90.

[24] C. Feng, Y. Wang, J. Zhang, L. Yu, D. Li, J. Yang, Z. Zhang, Appl. Catal. B- Environ. 113 (2012) 61–71.

[25] M. Zhang, Z. Jin, J. Zhang, X. Guo, J. Yang, W. Li, X. Wang, Z. Zhang, J. Mol. Catal. A: Chem. 217 (2004) 203–210.

[26] H. Lu, B. Zhao, R. Pan, J. Yao, J. Qiu, L. Luo, Y. Liu, RSC Adv. 4 (2014) 1128–1132.

[27] C. Yang, Z. Wang, T. Lin, H. Yin, X. Lu, D. Wan, T. Xu, C. Zheng, J. Lin, F. Huang, X. Xie, M. Jiang, J. Am. Chem. Soc. 135 (2013) 17831–17838.

[28] A. Naldoni, M. Allieta, S. Santangelo, M. Marelli, F. Fabbri, S. Cappelli, C.L. Bianchi, R. Psaro, V. Dal Santo, J. Am. Chem. Soc. 134 (2012) 7600–7603.

[29] G. Wang, H. Wang, Y. Ling, Y. Tang, X. Yang, R.C. Fitzmorris, C. Wang, J.Z. Zhang, Y. Li, Nano Lett. 11 (2011) 3026–3033.

[30] Z. Wang, C. Yang, T. Lin, H. Yin, P. Chen, D. Wan, F. Xu, F. Huang, J. Lin, X. Xie, M. Jiang, Adv. Funct. Mater. 23 (2013) 5444–5450.

[31] T. Xia, W. Zhang, J.B. Murowchick, G. Liu, X. Chen, Adv. Energy Mater. 3 (2013) 1516–1523.

[32] T. Xia, W. Zhang, J.B. Murowchick, G. Liu, X. Chen, Nano Lett. 13 (2013) 5289–5296.

[33] W. Wang, W. Huang, Y. Ni, C. Lu, Z. Xu, ACS Appl. Mater. Interfaces 6 (2013) 340–348.

[34] F. Zuo, K. Bozhilov, R.J. Dillon, L. Wang, P. Smith, X. Zhao, C. Bardeen, P. Feng, Angew. Chem. 124 (2012) 6327–6330.

[35] F. Zuo, L. Wang, T. Wu, Z. Zhang, D. Borchardt, P. Feng, J. Am. Chem. Soc. 132 (2010) 11856–11857.

[36] W. Zhuang, L. Li, J. Zhu, R. An, L. Lu, X. Lu, X. Wu, H. Ying, ChemElectroChem 2 (2015) 374–381.

[37] L. Li, K. Shi, R. Tu, Q. Qian, D. Li, Z. Yang, X. Lu, Chin. J. Catal. 36 (2015) 1943–1948.

[38] J. Wang, P. Liu, X. Fu, Z. Li, W. Han, X. Wang, Langmuir 25 (2009) 1218–1223.

[39] Y. Zhao, W. Ma, Y. Li, H. Ji, C. Chen, H. Zhu, J. Zhao, Angew. Chem. Int. Ed. Engl. 51 (2012) 3188–3192.

[40] M. Kong, Y. Li, X. Chen, T. Tian, P. Fang, F. Zheng, X. Zhao, J. Am. Chem. Soc. 133 (2011) 16414–16417.

[41] S. Chakraverty, S. Mitra, K. Mandal, P.M.G. Nambissan, S. Chattopadhyay, Phys. Rev. B 71 (2005) 0241151–0241158.